sensors

MDPI

Article

Fabrication of Ordered SnO_2 Nanostructures with Enhanced Humidity Sensing Performance

Wei Li [1,2,*], Juyan Liu [1], Chao Ding [1], Gang Bai [1], Jie Xu [1], Qingying Ren [1] and Jinze Li [1]

[1] College of Electronic and Optical Engineering, Nanjing University of Posts and Telecommunications, Nanjing 210023, China; 1215022733@njupt.edu.cn (J.L.); 1015020833@njupt.edu.cn (C.D.); Baigang@njupt.edu.cn (G.B.); jiexu@njupt.edu.cn (J.X.); Rqy@njupt.edu.cn (Q.R.); LiJinze@njupt.edu.cn (J.L.)

[2] State Key Laboratory of Millimeter Waves, Southeast University, Nanjing 210096, China

* Correspondence: Liw@njupt.edu.cn

Received: 19 September 2017; Accepted: 18 October 2017; Published: 20 October 2017

Abstract: Ordered SnO_2 nanostructures were prepared as humidity sensors by nanosphere lithography with the magnetron sputtering technique. The X-ray diffraction patterns of SnO_2 nanostructures show that all intense diffraction peaks correspond to the crystallographic planes of SnO_2. The Atomic Force Microscope (AFM) mage shows that these SnO_2 nanostructures exhibited a classic honeycomb structure. The resistance of this sensor was measured to show that the resistance of the sensor decreases with an increase from lower relative humidity (RH) to higher RH. Additionally, the longest response/recovery time was 32 s/42 s for 11–96% RH. The hysteresis for the SnO_2 nanostructure sensor was <5%.

Keywords: SnO_2 nanostructure; humidity sensor; nanosphere lithography

1. Introduce

Environmental pollution is currently becoming more and more serious. It does a great harm to human life. Thus, gas sensors have received much attention in recent years [1–9]. Humidity sensors are one of the most important sensors, and have been widely used in our day-to-day life. In contrast to other gas sensors, which are used to detect organic vapour gas and hazardous gas, a humidity sensor can provide useful information for health care, living comforts, cultural heritage protection, climate control in green houses, etc. All kinds of nanostructure materials have been extensively studied. Humidity sensors produced from metal oxide semiconductor materials, such as SnO_2 [10,11], WO_3 [12,13], and ZnO [14,15], have been applied in a variety of different areas.

SnO_2, a wide band gap (~3.7 eV) semiconductor that has unique electrical properties and high physical/chemical stability, is an important material in the field of humidity sensors [16,17]. Tomer et al. found that the SnO_2/SBA-15 nanocomposite prepared by in-situ method exhibits excellent sensitivity towards change in %RH, as well as good repeatability, short response/recovery time, negligible hysteresis, and great stability [18]. Georgieva and co-workers prepared nanosized thin SnO_2 layers doped with Te and TeO_2. This showed perfect humidity sensor characteristics, with very high sensitivity at room temperature, fast response and short recovery period, and good selectivity [19]. Feng et al. reported that SnO_2 nanostructures with different morphologies had been prepared by a one-step hydrothermal method. The nanosensor, based on 3D hierarchical SnO_2 dodecahedral nanocrystals, exhibited superior humidity-sensing properties [20]. These SnO_2 nanostructures are able to provide a regular porosity and a large specific surface area, permitting high accessibility for the water molecules and providing more active sites for the surface physical/chemical interaction between water molecules and the SnO_2 materials.

Here, we will introduce a successful attempt to synthesize ordered SnO_2 nanostructures by nanosphere lithography. The nanosphere lithography technique is an inexpensive and efficient method that has been reported for the fabrication of periodic nanostructures [21–23]. These nanostructures have a classic honeycomb structure, which can provide a much larger surface area, compared to bulk materials. In our previous work, it was reported that an ordered silicon nanopillar array prepared by nanoshpere lithography exhibited excellent humidity-sensing properties [24–26]. Here, the ordered SnO_2 nanostructure was studied as a new nanostructure material for gas sensors. Room temperature current sensitivity of the ordered SnO_2 nanostructures sensor was investigated at different values of relative humidity. The result shows that the SnO_2 nanostructure sensor has good sensing properties with high sensitivity, fast response and short recovery period, and low hysteresis.

2. Experiment

Our approach to production is shown in Figure 1. At first, a monolayer of polystyrene (PS) nanosphere with 220 nm in diameter was fabricated on Si substrate by self-assembly (Figure 1a). The self-assembly method was described in detail in our previous work [25]. Next, the prepared substrate with PS spheres was etched by reaction ion etching (RIE) with oxygen under these conditions: chamber pressure 1 Torr, RF power 20 W, O_2 flow 20 sccm, and etching time 30 s. O_2 plasma was applied to shrink the PS nanospheres (Figure 1b). Then, the SnO_2 film was coated on the PS colloid sphere array by using the magnetron sputtering technique (Figure 1c). The base pressure of the vacuum chamber was 2.0×10^{-4} Pa. The SnO_2 target, with 99.99% purity, was purchased from Beijing Goodwill Metallic Technology Co. The sputtering machine was set to a power of 90 mW, a current of 140 mA, and a 2 min deposition time. During the film deposition, the distance between the PS colloid sphere array substrate and the SnO_2 target was 20 cm. After sputtering, the sample was put into a solvent, such as methanol or tetrahydrofuran (THF), to remove the PS nanospheres. Then, an ordered SnO_2 nanostructure was obtained. Subsequently, the performance of thermal annealing for SnO_2 nanostructure was taken at 1000 °C with oxygen for 1 h. Finally, the fork-shaped electrodes were prepared by electron-beam evaporation (EBV) on the SnO_2 nanostructure surface. The electrode width and separation distance was 2 mm (Figure 1e).

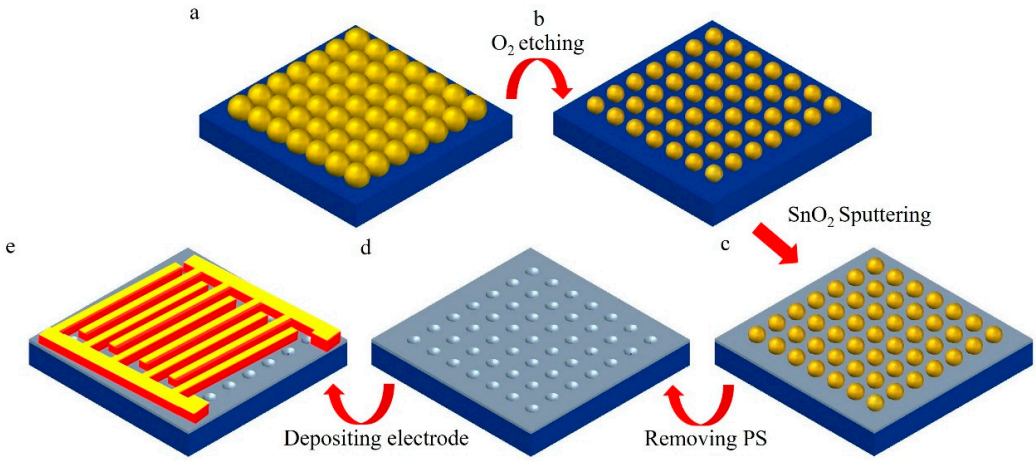

Figure 1. The schematics of the procedure for fabricating the SnO_2 nanostructure. (**a**) A monolayer of polystyrene nanosphere was fabricated on Si substrate by self-assembly. (**b**) The nanospheres were etching by O_2. (**c**)The SnO_2 was sputtering. (**d**) The nanospheres were removed. (**e**) The fork-shaped electrodes were prepared by electron-beam evaporation.

The humidity environments were provided by using self-made air-tight glass chambers containing a series of standard aqueous salt solutions (LiCl, $Mg(NO_3)_2$, $MgCl_2$, NaCl, KCl and KNO_3), with the RH being about 11%, 33%, 54%, 75%, 84%, and 96%, respectively. The electrical resistance was

monitored by using an Agilent (B1505A) electrometer. All the measurements were carried out under atmospheric pressure and at 25 °C.

3. Results and Discussions

Figure 2 shows the X-ray diffraction patterns of ordered SnO_2 nanostructure film. Curve a represents the sample with thermal annealing, and curve b is for the sample without thermal annealing. As seen in this figure, nine well-resolved peaks were obtained at 26.8°, 34.4°, 38.1°, 52.4°, 54.9°, 62.3°, 64.6°, 66.1° and 71.8°, corresponding to (110), (101), (200), (211), (220), (310), (112), (301) and (202) planes of SnO_2, respectively. Furthermore, the full width at half maximum (FWHM) of peak is reduced after thermal annealing. According to the Scherrer equation:

$$D = k\lambda / \beta \cos\theta,$$

the size of SnO_2 nanoparticles is increased after thermal annealing. Here, D is the size of nanoparticles, k is the Scherrer constant, λ is the X-ray wavelength, β is the FWHM and θ is the angle of diffraction.

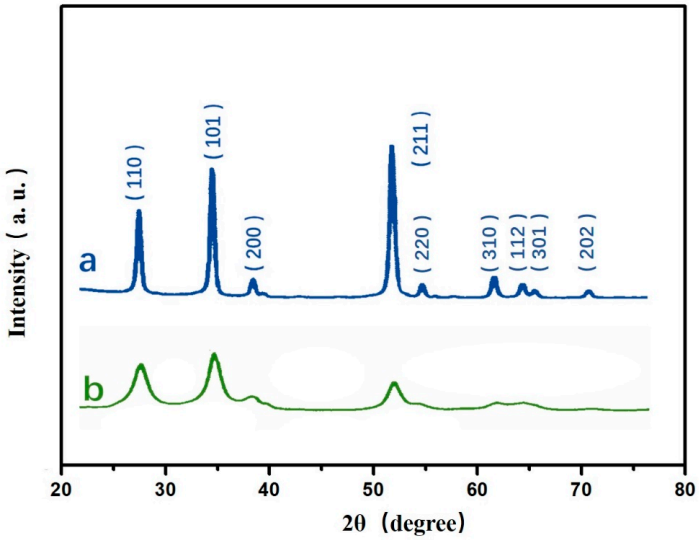

Figure 2. The XRD patterns of SnO_2 nanostructure film. (a) The SnO_2 after thermal annealing; (b) as-deposited.

Figure 3a is the oblique view of AFM image of the SnO_2 nanostructure. It is shown that the classic honeycomb ordered SnO_2 nanostructure has been obtained. The period was 220 ± 10 nm, the same as the PS nanosphere size. From Figure 3b, the thickness of the SnO_2 nanostructure can be seen to be 30 ± 5 nm, and the size of SnO_2 nanoparticles was 170 ± 10 nm. In the sputtering process, the SnO_2 film is deposited on the close-packed PS nanosphere array along the perpendicular direction, forming a nanocap array. Meanwhile, the SnO_2 nanoparticles are able to penetrate the interstice among the three nearest-neighboring PS nanospheres to reach the silicon wafer substrate, creating triangular-shaped SnO_2 nanoparticle arrays. After removing PS nanospheres, only ordered triangular-shaped SnO_2 nanoparticles are left on the silicon substrate.

Figure 4a,b shows a resistive-type humidity sensor based on ordered SnO_2 nanostructures with applied voltage from 1 V to 3 V. It clearly reveals that the resistance of the sensor decreases with an increase from lower RH to higher RH. Figure 4c shows the R-V curves of the SnO_2 nanostructure at different RHs. It shows a good linear behaviour, which proves that Ohmic laws apply well in this case. By calculation, it was determined that the resistance of this sensor is about 6.54×10^9 Ω at 11% RH, which is 18 times that of 0.36×10^9 Ω at 75% RH and 595 times that of 0.011×10^9 Ω at 96% RH. This proves that water vapour has a strong influence on the conductivity of ordered SnO_2

nanostructure-based humidity sensors. As observed, the resistance exhibits a large change at RH 75%, which means that more water vapour has been absorbed. In this sensor, the adsorption of water vapour on the surface of SnO_2 nanostructure sensor is mainly due to the large surface area of the ordered classic honeycomb nanostructure, which is shown in Figure 3a. It is well known that the chemically absorbed oxygen ion (O_2^-) is stable on the SnO_2 surface at room temperature, due to the adsorption energy [27]. The adsorbed oxygen ion on the surface of SnO_2 nanostructure has been replaced by competitive water molecule absorption. At higher RH, water molecules start to condense, which contributes to the limited surface diffusion of the water molecules. As a result, the depletion layer becomes more and more thin, and the conductivity of the SnO_2 nanostructure surface increases [28].

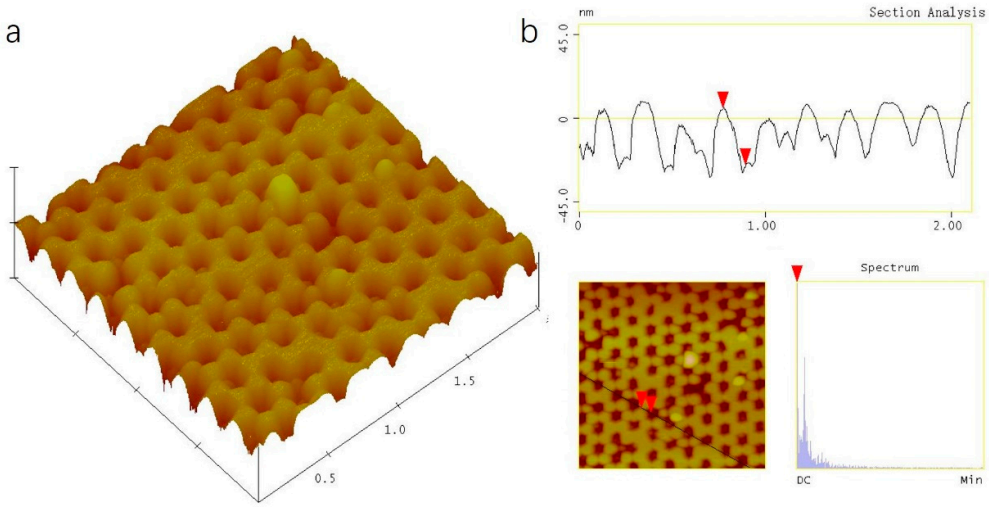

Figure 3. (**a**)The AFM image of SnO_2 nanostructure. (**b**)The section analysis of SnO_2 nanostructure.

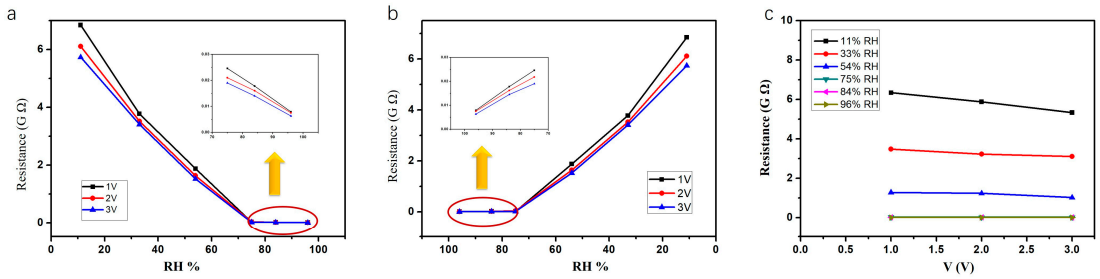

Figure 4. Plot of resistance response of SnO_2 nanostructures with humidity from 11% to 96% (**a**), and from 96% to 11% (**b**). (**c**) The R-V curves of the SnO_2 nanostructure with different RHs.

$K(RH) = (R_1 - R_2)/R_1$ is defined as the sensitivity when the applied voltage is 1 V, where R_2 is the electric resistance at the current humidity and R_1 is the electric resistance at 11% RH. We also examined the plane substrate as a comparison. Figure 5 shows the relation between sensitivity and relative humidity for the nanostructure and the plane substrate. Obviously, the sensitivity of the nanostructure substrate is better than that of the plane substrate. As seen in Figure 5, the SnO_2 nanostructure sensor has good sensing properties and shows good linearity with relative humidity at humidity variations between 11% RH and 75% RH. The response and recovery time under different humidity levels was studied, and the results are shown in Figure 6. By measuring, it was found that the average response/recovery times are 18 s/25 s for 11–33% RH, 25 s/33 s for 11–54% RH, 32 s/42 s for 11–96% RH. Table 1 shows the detailed results for the response and recovery time. It was found that the response/recovery time increased with increasing RH, and the remains approximately constant above 75% RH. The average values are 31 s for response time and 40 s for recovery time. It is due to

that the surface area was increased by about 50% for this quasi-identical and ordered nanostructure. On the other hand, this provided an effective channel for the absorption and desorption of water molecules. As a result, fast response and recovery times were obtained.

The hysteresis is an important characteristic of the humidity sensor. Figure 7 shows the hysteresis curve in the process of adsorption and desorption. The lower curve represents the increasing RH (adsorption) process, and the upper curve represents the decreasing RH (desorption) process. As seen in Figure 7, the two curves are very close. The maximum humidity hysteresis is less than 5% at 96% RH, which indicates that the hysteresis for the SnO_2 nanostructure sensor is small.

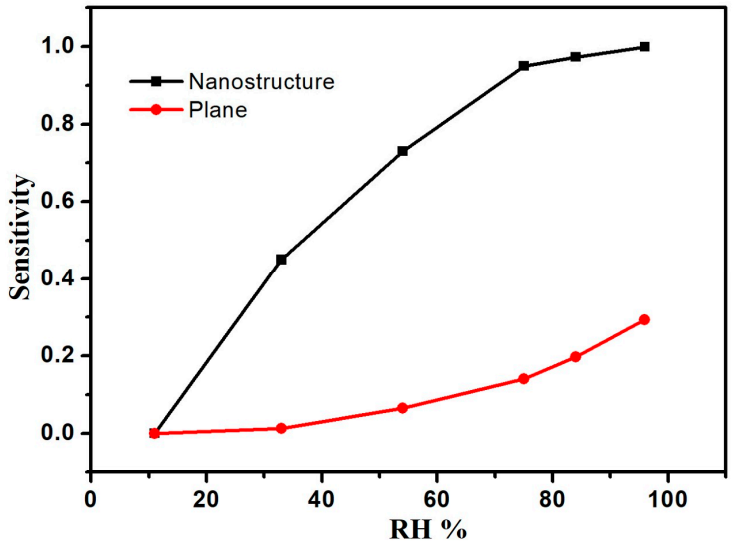

Figure 5. The relation between sensitivity and relative humidity with nanostructure and plane substrate.

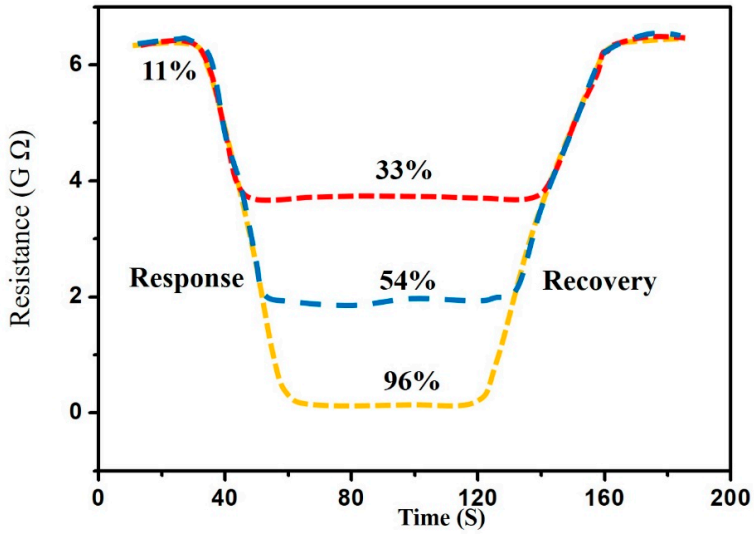

Figure 6. Response/recovery time of the SnO_2 nanostructure sensor from 11% RH to 96% RH.

Table 1. The response/recovery time of the SnO_2 nanostructure sensor.

RH	11–33%	11–54%	11–75%	11–84%	11–96%
Response time (s)	18	25	30	31	32
Recovery time (s)	25	33	39	40	42

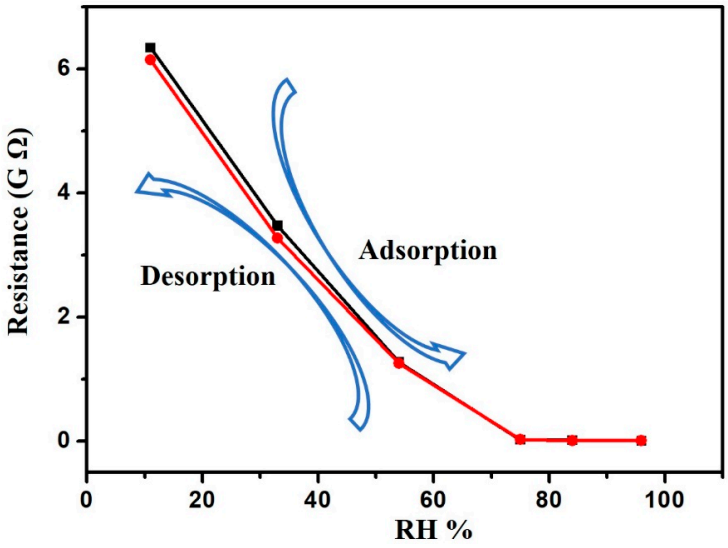

Figure 7. The hysteresis curve showing adsorption/desorption responses.

4. Conclusions

In conclusion, ordered SnO_2 nanostructures as humidity sensors were fabricated by nanosphere lithography with the magnetron sputtering technique. The resistance of this sensor was measured to show the humidity sensitivity. The results demonstrate that the resistance of the sensor decreases with an increase from lower RH to higher RH. The SnO_2 nanostructure sensor has good sensing properties and shows good linearity with relative humidity. The longest response/recovery time is 32 s/42 s at humidity variation between 11% RH and 96% RH. The hysteresis of the SnO_2 nanostructure sensor is less than 5%. These results are due to the large surface area of classic honeycomb ordered nanostructures.

Acknowledgments: This work is supported by National Natural Science Foundation of China (Nos. 11504177, 51602159), Natural Science Foundation of Jiangsu Province (Nos. BK20160909, BK20171442), the Open Foundation of State Key Laboratory of Millimeter Waves of Southeast University (K201723).

Author Contributions: W.L. and J.L. conceived and designed the experiments; C.D. and J.X. performed the experiments; Q.R and Z.L analysed the data; W.L and G.B wrote the paper.

Conflicts of Interest: The authors declare no conflict of interest.

References

1. Kong, J.; Franklin, N.R.; Zhou, C.; Chapline, M.G.; Peng, S.; Cho, K.; Dai, H. Nanotube Molecular Wires as Chemical Sensors. *Science* **2000**, *287*, 622–625. [CrossRef] [PubMed]
2. Borini, S.; White, R.; Wei, D.; Astley, M.; Haque, S.; Spigone, E.; Harris, N.; Kivioja, J.; Ryhanen, T. Ultrafast Graphene Oxide Humidity Sensors. *ACS Nano* **2013**, *7*, 11166–11173. [CrossRef] [PubMed]
3. Wang, Y.; Park, S.; Yeow, J.T.W.; Langner, A.; Müller, F. A capacitive humidity sensor based on ordered macroporous silicon with thin film surface coating. *Sens. Actuators B Chem.* **2010**, *149*, 136–142. [CrossRef]
4. Choi, K.; Hwang, S.J.; Dai, Z.; Kang, Y.C.; Lee, J.H. Rh-catalyzed WO_3 with anomalous humidity dependence of gas sensing characteristics. *RSC Adv.* **2014**, *4*, 53130–53136. [CrossRef]
5. Liu, X.; Wang, R.; Zhang, T.; He, Y.; Tu, J.; Li, X. Synthesis and characterization of mesoporous indium oxide for humidity sensing applications. *Sens. Actuators B Chem.* **2010**, *150*, 442–448. [CrossRef]
6. Da Silva, L.F.; M'Pekob, J.C.; Ariadne, C.C.; Bernardini, S.; Mastelaro, V.R.; Aguir, K.; Ribeiro, C.; Longo, E. UV-enhanced ozone gas sensing response of ZnO-SnO_2 heterojunctions at room temperature. *Sens. Actuators B Chem.* **2017**, *240*, 573–579. [CrossRef]
7. Jha, R.K.; Guha, P.K. Liquid exfoliated pristine WS_2 nanosheets for ultrasensitive and highly stable chemiresistive humidity sensors. *Nanotechnology* **2016**, *27*, 475503. [CrossRef] [PubMed]

8. Duy, T.P.; Chung, G.S. Effects of rapid thermal annealing on humidity sensor based on graphene oxide thin films. *Sens. Actuators B Chem.* **2015**, *220*, 1050–1055.
9. Rimeika, R.; Čiplys, D.; Poderys, V.; Rotomskis, R.; Shur, M.S. Fast-response and low-loss surface acoustic wave humidity sensor based on bovine serum albumin-gold nanoclusters film. *Sens. Actuators B Chem.* **2017**, *239*, 352–357. [CrossRef]
10. Karthick, S.; Lee, H.S.; Kwon, S.J.; Natarajan, R.; Saraswathy, V. Standardization, Calibration, and Evaluation of Tantalum-Nano rGO-SnO_2 Composite as a Possible Candidate Material in Humidity Sensors. *Sensors* **2016**, *16*, 2079. [CrossRef] [PubMed]
11. Song, X.; Qi, Q.; Zhang, T.; Wang, C. A humidity sensor based on KCl-doped SnO_2 nanofibers. *Sens. Actuators B Chem.* **2009**, *138*, 368–373. [CrossRef]
12. Tomer, V.K.; Duhan, S. Highly sensitive and stable relative humidity sensors based on WO_3 modified mesoporous silica. *Appl. Phys. Lett.* **2015**, *106*, 063105. [CrossRef]
13. Staerz, A.; Berthold, C.; Russ, T. The oxidizing effect of humidity on WO_3 based sensors. *Sens. Actuators B Chem.* **2016**, *237*, 54–58. [CrossRef]
14. Hsu, C.L.; Su, I.L.; Hsueh, T.J. Tunable Schottky contact humidity sensor based on S-doped ZnO nanowires on flexible PET substrate with piezotronic effect. *J. Alloy. Compd.* **2017**, *705*, 722–733. [CrossRef]
15. Mahjoub, M.A.; Monier, G.; Robert-Goumet, C. Synthesis and Study of Stable and Size-Controlled ZnO-SiO_2 Quantum Dots: Application as a Humidity Sensor. *J. Phys. Chem. C* **2016**, *120*, 11652–11662. [CrossRef]
16. Lopez-Torres, D.; Elosua, C.; Villatoro, J.; Zubia, J.; Rothhardt, M.; Schuster, K.; Arregui, F.J. Enhancing sensitivity of photonic crystal fiber interferometric humidity sensor by the thickness of SnO_2 thin films. *Sens. Actuators B Chem.* **2017**, *251*, 1059–1067. [CrossRef]
17. Zhang, D.; Sun, Y.E.; Li, P.; Zhang, Y. Facile Fabrication of MoS_2-Modified SnO_2 Hybrid Nanocomposite for Ultrasensitive Humidity Sensing. *ACS Appl. Mater. Interfaces* **2016**, *8*, 14142–14149. [CrossRef] [PubMed]
18. Tomer, V.K.; Duhan, S. In-situ synthesis of SnO_2/SBA-15 hybrid nanocomposite as highly efficient humidity sensor. *Sens. Actuators B Chem.* **2015**, *212*, 517–525. [CrossRef]
19. Georgieva, B.; Podolesheva, I.; Spasov, G.; Pirov, J. Nanosized Thin SnO_2 Layers Doped with Te and TeO_2 as Room Temperature Humidity Sensors. *Sensors* **2014**, *14*, 8950–8960. [CrossRef] [PubMed]
20. Feng, H.L.; Li, C.; Li, T.; Diao, F.; Xin, T.; Liu, B.; Wang, Y. Three-dimensional hierarchical SnO_2 dodecahedral nanocrystals with enhanced humidity sensing properties. *Sens. Actuators B Chem.* **2017**, *243*, 704–714. [CrossRef]
21. Li, W.; Wang, S.L.; He, S.F.; Wang, J.; Guo, Y.; Guo, Y. Enhanced photoluminescence from CdS with SiO_2 nanopillar arrays. *Sci. Rep.* **2015**, *5*, 11375. [CrossRef] [PubMed]
22. Rybczynski, J.; Ebels, U.; Giersig, M. Large-scale, 2D arrays of magnetic nanoparticles. *Colloid Surf. A* **2003**, *219*, 1–6. [CrossRef]
23. Li, W.; Wang, S.L.; Hu, M.Y.; He, S.; Ge, P.; Wang, J.; Guo, Y.Y.; Zhaowei, L. Enhancement of electroluminescence from embedded Si quantum dots/SiO_2 multilayers film by localized-surface-plasmon and surface roughening. *Sci. Rep.* **2015**, *5*, 11881. [CrossRef] [PubMed]
24. Li, W.; Hu, M.Y.; Ge, P.P.; Wang, J.; Guo, Y. Humidity sensing properties of morphology-controlled ordered silicon nanopillar. *Appl. Surf. Sci.* **2014**, *317*, 970–973. [CrossRef]
25. Li, W.; Dai, E.; Bang, G.; Xu, J. Depth-dependent humidity sensing properties of silicon nanopillar array. *Sens. Actuators B Chem.* **2016**, *237*, 526–533. [CrossRef]
26. Li, W.; Feng, Z.; Dai, E.; Xu, J.; Bai, G. Organic vapour sensing properties of area-ordered and size-controlled silicon nanopillar. *Sensors* **2016**, *16*, 1880. [CrossRef] [PubMed]
27. Morrison, S.R. *The Chemical Physics of Surfaces*; Plenum Press: New York, NY, USA, 1977.
28. Li, L.; Wu, K.; Wang, Y.; Zhu, Z. Structure and humidity sensing properties of SnO_2 zigzag belts. *Cryst. Res. Technol.* **2010**, *45*, 539–544. [CrossRef]